Using CloudSat and the A-Train for Model Evaluation

Matthew Lebsock, Kenta Suzuki and Graeme Stephens

*Jet Propulsion Laboratory, California Institute of Technology,
Pasadena CA*

Abstract

Coincident observations cloud and precipitation from CloudSat and MODIS permit a more detailed evaluation of precipitation processes than has previously been possible from satellite observations. Here we present several new diagnostics of the hydrologic cycle focused on warm rain, which are facilitated by these state of the art observations. These diagnostics demonstrate the propensity of models to produce precipitation that is too frequent and too light and further provides insight into inaccuracies in the representation of physical processes (autoconversion and accretion) that govern the precipitation efficiency.

1. CloudSat Precipitation

CloudSat offers a view of global precipitation, which complements that of more traditional climatologies such as the Global Precipitation Climatology Project (GPCP). This is because of the unique sensitivity of the Cloud Profiling Radar to the occurrence of precipitation, including light precipitation and snow that go undetected by the standard remote sensing methods. Precipitation algorithms for CloudSat have developed and are outlined in a series of papers [*L'Ecuyer and Stephens*, 2002; *Haynes et al.*, 2009; *Lebsock and L'Ecuyer*, 2011]. Figures 1 and 2 depict the climatology of the probability of precipitation and the quantification of warm rain from CloudSat. Note the high frequency of occurrence of precipitation in the high latitudes and warm rain in the subtropical eastern ocean basins. Also note the accumulation of surface rainfall from warm rain clouds approaching 1 mmd^{-1} in the subtropics. These are new metrics for model evaluation that can be used in conjunction with the standard precipitation diagnostics.
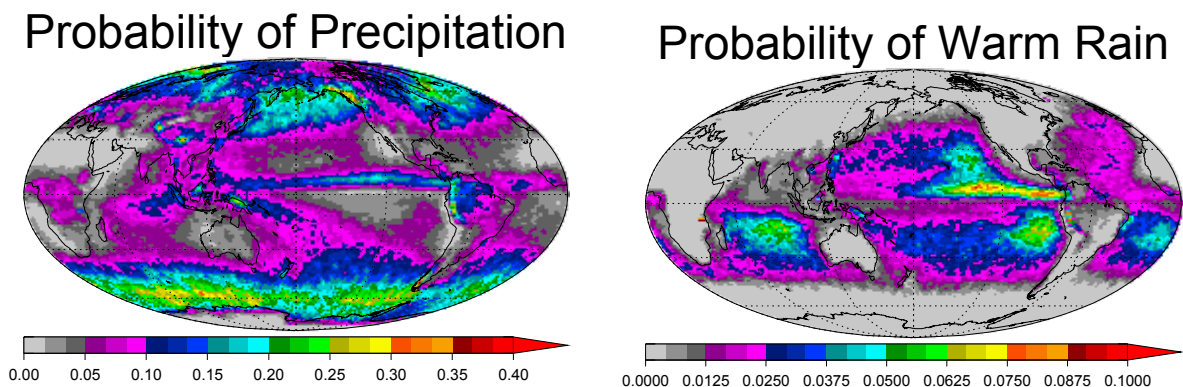

Figure 1: The probability of surface precipitation of any phase (left panel) and from clouds with cloud top temperatures warmer than 273 K (right panel) as derived from the CloudSat algorithms.
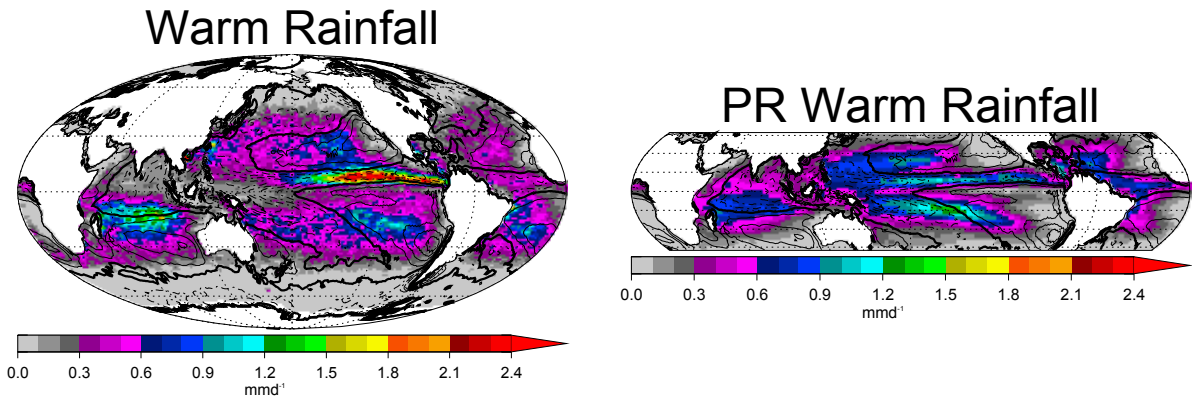
Figure 2 : The mean precipitation rate from warm rain clouds with cloud top temperaures greater than 273 K derived from CloudSat (left panel) and the TRMM Precipitation Radar (right panel).

2.   Multi-Sensor Metrics

Coincident observations of cloud from MODIS and precipitation from CloudSat permit a more complete evaluation of model performance. In particular diagnostics that use both pieces of information simultaneously can provide guidance on particular parameterization that are deficient in the model.
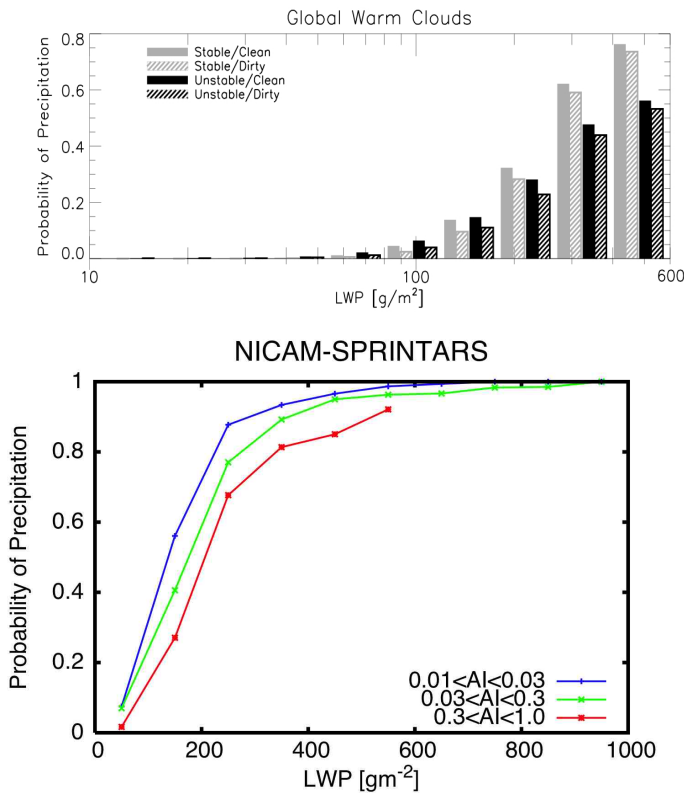

Figure 3: The probability of precipitation from CloudSat as a function of the MODIS cloud water path (top; adopted from [Lebsock et al., 2008]). Similar statistics derived from the NICAM model run at 7km resolution and screened for low cloud scenarios (bottom). The 'clean' and 'dirty' labels are based on the MODIS aerosol index (the product of aerosol optical depth and angstrom exponent). The 'stable' and 'unstable' labels are based on the potential temperature difference between the surface and 700 hPa. See [Lebsock et al., 2008] for further details.

A straightforward example of this sensor synergy is shown in Figure 3, which shows the probability of precipitation as a function of the cloud water path from both observations and a model simulation from a NICAM model simulation. The model shows a qualitatively similar dependence of the probability of precipitation on both the water path and on the aerosol burden, however it has a tendency to produce precipitation too quickly hinting at an overly aggressive auto-conversion parameterization.

A more detailed diagnostic is provided by the Contoured Frequency by Optical Depth Diagrams (CFODD) introduced by [*Suzuki et al.*, 2010]. These diagrams show the statistics of the profile of radar reflectivity stratified by the observed optical depth as a function of various observed cloud droplet effective radii. Because of the sensitivity of MODIS to cloud and CloudSat reflectivities to precipitation the CFODD offers a fingerprint of the water conversion process from cloud to precipitation. An example of the CFODD is provided in Figure 4.
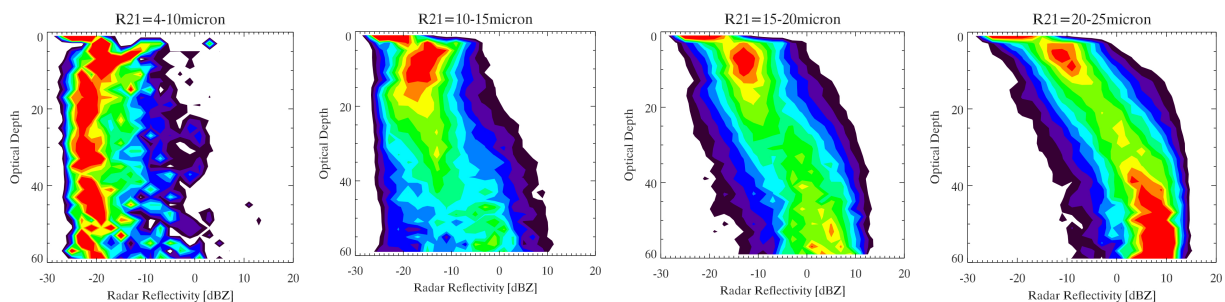

Figure 4: A Contoured Frequency by Optical Depth Diagram. Each panel shows a grouping based on the retrieved MODIS effective radius. The reflectivity profile is indicative of the intensity of the precipitation. The lowest effective radii bin has a vertically oriented profile that is suggestive of non-precipitating clouds. As the effective radius increases the profile becomes bottom heavy suggesting precipitation.

3.   Evaluation of Sub-grid Microphysical Correlations

This section focuses on two particular microphysical processes that govern the generation of precipitation in warm boundary layer clouds: (1) autoconversion: the direct collision and coalescence of cloud droplets into embryonic precipitation drops and (2) accretion: the collection of cloud droplets by falling precipitation drops. Together these two processes determine the overall coalescence efficiency in warm clouds and thus have a large influence on the timescale of precipitation. The rates at which these processes occur on local scales (i.e. scales smaller than the model resolution) are generally approximated by non-linear power-law equations in the microphysical variables of cloud water mixing ratio (q_c), precipitation water mixing ratio (q_p) and cloud droplet number concentration (N_c). In principle, to calculate the process rates, one would want to know the sub-grid variability of the microphysical quantities (q_c, q_p, N_c) and the co-variability of these quantities. However, the standard method to address the dilemma of sub-grid variability is the arbitrary 'tuning' of the parameters that govern the microphysical process rates. While uncertainty exists in the value of these parameters thus justifying some degree of tuning, it is not uncommon that they must be tuned well outside their known range of variability to obtain reasonable model simulations.

The intent of this section is two-fold. First, we introduce a simple analytic framework in which to describe the sub-grid covariance between cloud and precipitation water and examine the effect of

including covariance on the modeled accretion rates. We highlight the fact that neglecting covariance between cloud and precipitation causes a systematic underestimate of accretion rates. Second, we present observational constraints on sub-grid cloud and precipitation distributions from satellite observations and explore their scale-dependence. These constraints are presented in a form that is consistent with the analytic construct and could be readily adapted by existing cloud microphysics parameterizations.

3.1. Mathematical Constructs

3.1.1. A Measure of Sub-grid Variability

We use as a measure of sub-grid variability of a generic parameter (x) the inverse normalized variance,

$$v_x = \frac{\bar{x}^2}{\sigma^2} \tag{1}$$

where the overbar denotes the conditional ('in cloud') grid mean and σ is the standard deviation of x. The variable (v) is also often referred to as homogeneity, because large values of v are indicative of homogenous distributions whereas low values are indicative of heterogeneous distributions. In the context of process parameterizations in global models, v has been used to characterize the variability of cloud optical depth [*Barker et al.*, 1996] and cloud water [*Wood and Hartmann*, 2006]. Distinct variations in this parameter are observed with cloud fraction and type [*Pincus et al.*, 1999]. For example, overcast stratus cloud is more likely to have larger values of v than those of scattered cumulus.

3.1.2. Representation of the Microphysical Process Rates

The rates at which accretion (M_{ac}) and autoconversion (M_{au}) occur are generally approximated by non-linear power-law equations of the form,

$$M_{ac} = a_{ac} \left(q_c q_p \right)^{b_{ac}} \tag{2}$$

$$M_{au} = a_{au} q_c^{b_{au,q}} N_c^{b_{au,N}} \tag{3}$$

The a's and b's are coefficients and the b's represent the degree to which each process is non-linear and thus influenced by sub-grid variability. In general, the autoconversion formulation is more non-linear than the accretion formulation ($b_{au,q} > b_{ac}$) and is therefore thought to be more susceptible to sub-grid scale biases. Note also that the accretion rate is determined as the product of q_p and q_c and thus influenced by the covariance of these parameters. In this work we will use the power-law coefficients given by *Khairoutdinov and Kogan* [2000].

3.1.3. Sub-grid Distribution Functions and Process Rate Enhancement Factors

One approach to modeling sub-grid scale effects is through a Probability Density Function (PDF) approach, in which the PDFs of the microphysical quantities may be either predicted or prescribed. An advantage of the PDF approach is that it permits the tuning of the process rates through a traceable and physically meaningful assumption regarding the sub-grid distribution of microphysical properties

without resorting to arbitrary tuning of the process rate power law parameters (*a*'s and *b*'s) outside of physically reasonable bounds.

In the context of modeling sub-grid scale effects on microphysical process rates, the PDF of cloud water is often approximated by the univariate normalized gamma distribution [*Pincus and Klein*, 2000; *Morrison and Gettelman*, 2008]. In this work we will follow an alternative formulation of *Larson and Griffin* [2012] who adopt the log-normal distribution to represent the sub-grid distribution of the microphysical parameters. The univariate lognormal distribution of any quantity (*x*) is given by,

$$P(x) = \frac{1}{\sqrt{2\pi} x \sigma_{ln}} \exp\left(\frac{(\ln(x) - \mu)^2}{2\sigma_{ln}^2}\right) \tag{4}$$

where μ and σ_{ln} are the mean and standard deviation of ln(*x*). However Eqns. 1 and 2 are functions of products of microphysical variables and therefore require a description of the sub-grid covariance of these parameters. To account for this covariance a bivariate distribution is required. The analogous bivariate lognormal distribution of any two quantities (*x_1*,*x_2*) is given by,

$$P(x_1, x_2) =$$

$$\frac{1}{\sqrt{2\pi}\sigma_{ln,1}\sigma_{ln,2}x_1 x_2 \sqrt{1-\rho^2}} \exp\left(\frac{(\ln(x_1)-\mu_1)^2}{2(1-\rho^2)\sigma_{ln,1}^2}\right) \exp\left(\frac{(\ln(x_2)-\mu_2)^2}{2(1-\rho^2)\sigma_{ln,2}^2}\right) \exp\left(\frac{\rho(x_1-\mu_1)(x_2-\mu_2)}{(1-\rho^2)\sigma_{ln,1}\sigma_{ln,2}}\right) \tag{5}$$

where ρ is the correlation coefficient between *x_1* and *x_2*.

With the assumption of a univariate lognormal distribution of a microphysical quantity (*x*) and that variations in *x* dominate the sub-grid effects on the process rates one may find the grid mean process rate for an arbitrary process following a power law of the form $M = ax^b$ by integrating the rate equation over the distribution [*Boutle et al.*, 2012],

$$\bar{M} = \int ax^b P(x)dx = E[v_x, b]a\bar{x}^b \tag{6}$$

where,

$$E[v_x, b] = \left(1 + \frac{1}{v_x}\right)^{\frac{b^2-b}{2}} \tag{7}$$

In the more general case of covariance between microphysical quantities where the process rate follows a power law form of $M = ax_1^{b_1}x_2^{b_2}$, a double integration over the microphysical distributions yields the grid mean process rate [*Boutle et al.*, 2012],

$$\bar{M} = \iint ax_1^{b_1}x_2^{b_2}P(x_1, x_2)dx_1 dx_2 = E^*[v_1, v_2, b_1, b_2, \rho]a\overline{x_1}^{b_1}\overline{x_2}^{b_2} \tag{8}$$

where,

$$E^*\left[v_1,v_2,b_1,b_2,\rho\right]=\left(1+\frac{1}{v_1}\right)^{\frac{b_1^2-b_1}{2}}\left(1+\frac{1}{v_2}\right)^{\frac{b_2^2-b_2}{2}}\exp\left(\rho b_1 b_2\sqrt{\ln\left(1+\frac{1}{v_1}\right)\ln\left(1+\frac{1}{v_2}\right)}\right) \qquad (9)$$

In this work we focus on the covariance of cloud and precipitation water and assume a uniform distribution of droplet number. Therefore Eqns. 6 and 7 apply to the assumptions that we have made regarding the autoconversion process (variable q_c and uniform N_c) and Eqns. 8 and 9 apply to the assumptions that we have made regarding the accretion process (variable q_c and q_p).

The form of Eqns. 6-9 is appealing because it allows the calculation of a grid mean process rate using the unmodified process rate coefficients applied to the grid mean microphysical variables. All sub-grid effects are contained in the enhancement factors E and E^*. Each of these factors may be tuned, however, this framework provides a convenient separation of the tuning that can be attributed to sub-grid influence and that related to the uncertainty in the process rate coefficients themselves. Furthermore, Eqn. 9 is satisfying in that it accounts for the likely possibility of correlation between microphysical parameters. From this equation it is clear that the three parameters that fundamentally determine the sub-grid influence on a process rate with known power law exponents (b_1 and b_2) are the normalized variances of the microphysical variables and the correlations between these variables (v_1, v_2, ρ). This equation is specific to the assumption of lognormally distributed variables, however these three fundamental parameters may be more generally applied to any assumed distribution function.

3.2. Observational Analysis

The parameters (v_1, v_2, ρ) are estimated for warm clouds over the ocean using observations from CloudSat and MODIS at various spatial resolutions approximating model grid boxes of differing sizes. Results shown here correspond to model grid boxes of size 141 km. The sample volume corresponds to a satellite footprint of approximately 1.5 km diameter. Note that estimation of these parameters is a function of the sample volume with small-scale sampling being preferable. However the satellite observations can provide us with the regional pattern of these parameters, which is difficult from high resolution modelling or in-situ data.

Figure 5 shows the histogram of the observed covariance parameters and Figure 6 shows their geographical distributions. The mediaan values of cloud precipitation correlation is 0.58. The median of the cloud and precipitation homogeneity are 2.46 and 1.51 respectively. These results demonstrate the unsurprising results that precipitation is more variable than cloud water and that the spatial correlation between these parameters is generally observed to be large. More importantly a coherent spatial distribution of the covariance parameters is discernable. Relatively larger correlations and parameter variance is observable in areas of frequent cumulus than in areas characterized by stratocumulus. These patterns influence the regional distributions of the sub-grid influence on the microphysical process rates. Most models have no physical mechanism for producing this sort of regionality. These particular observations offer a guide for model development that seeks to introduce a regional depiction of sub-grid variability in microphysics.

(A)
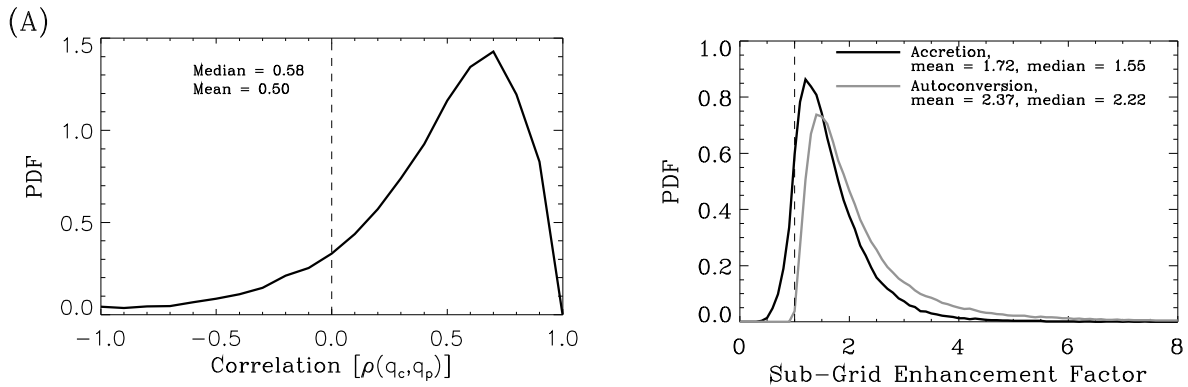
(B)

Figure 5: The histograms of the cloud-precipitation correlation (left) and the cloud and precipitation homogeneity (right) derived from CloudSat and MODIS.
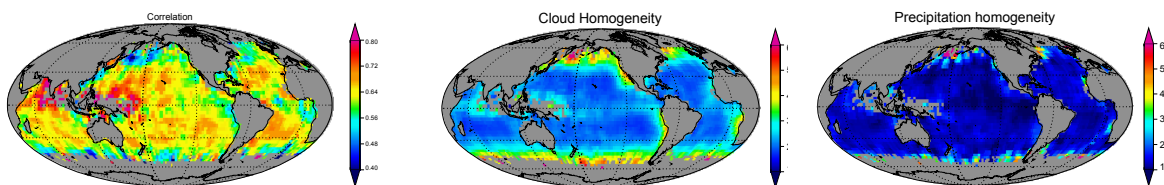

Figure 6: Regional distributions of the cloud-precipitation correlation (left) and the cloud and precipitation homogeneity (right) derived from CloudSat and MODIS.

Figure 7 shows the regional distribution of the enhancement factor for autoconversion and accretion derived from Figure 6. As a reminder the magnitude of these factors are dependent on the ~1.5 km sampling volume of this analysis, however the geographical distribution is not necessarily limited in the same manner. The autoconversion enhancement is approximately double that of the accretion enhancement regardless of location. Two regimes are evident in this figure: A shallow convective region characterized by low cloud water homogeneity, accretion enhancement near 80%, and autoconversion enhancement near 140%; A stratocumulus region in the eastern subtropical ocean basins and high-latitudes characterized by high homogeneity, accretion enhancement near 40%, and autoconversion enhancement near 60%. The regional variation in the enhancement factors is largely determined by the spatial distribution of the cloud homogeneity relative to that of the correlation. These results suggest that ρ might reasonably be parameterized as a global constant. Furthermore, if a parameterization hopes to achieve the correct regionality of process rate enhancement the most critical parameter to characterize is v_c, which fortunately can be evaluated from a number of existing observational datasets.
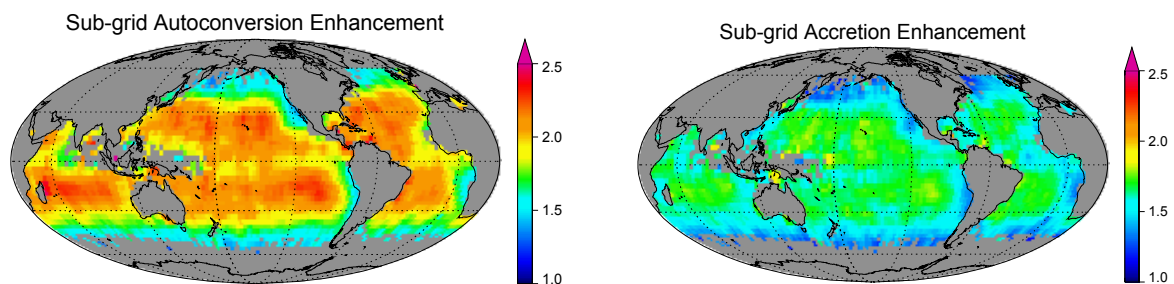

Figure 7: Regional distributions of the autoconversion (left) and accretion (right) enhancement factors derived from the results shown in figure 6.

4. References

Barker, H. W., B. A. Wiellicki, and L. Parker (1996), A Parameterization for Computing Grid-Averaged Solar Fluxes for Inhomogeneous Marine Boundary Layer Clouds. Part II: Validation Using Satellite Data, *Journal of the Atmospheric Sciences*, *53*(16), 2304–2316, doi:10.1175/1520-0469(1996)053<2304:APFCGA>2.0.CO;2.

Haynes, J. M., T. S. L'Ecuyer, G. L. Stephens, S. D. Miller, C. Mitrescu, N. B. Wood, and S. Tanelli (2009), Rainfall retrieval over the ocean with spaceborne W-band radar, *J. Geophys. Res.*, *114*(D8), D00A22, doi:10.1029/2008JD009973.

Khairoutdinov, M., and Y. Kogan (2000), A New Cloud Physics Parameterization in a Large-Eddy Simulation Model of Marine Stratocumulus, *Monthly Weather Review*, *128*(1), 229–243, doi:10.1175/1520-0493(2000)128<0229:ANCPPI>2.0.CO;2.

L'Ecuyer, T. S., and G. L. Stephens (2002), An Estimation-Based Precipitation Retrieval Algorithm for Attenuating Radars, *Journal of Applied Meteorology*, *41*(3), 272–285, doi:10.1175/1520-0450(2002)041<0272:AEBPRA>2.0.CO;2.

Larson, V. E., and B. M. Griffin (2012), Analytic upscaling of a local microphysics scheme. Part I: Derivation, *Quarterly Journal of the Royal Meteorological Society*, n/a–n/a, doi:10.1002/qj.1967.

Lebsock, M. D., and T. S. L'Ecuyer (2011), The retrieval of warm rain from CloudSat, *J. Geophys. Res.*, *116*(D20), D20209, doi:10.1029/2011JD016076.

Lebsock, M. D., G. L. Stephens, and C. Kummerow (2008), Multisensor satellite observations of aerosol effects on warm clouds, *J. Geophys. Res.*, *113*(D15), D15205, doi:10.1029/2008JD009876.

Morrison, H., and A. Gettelman (2008), A New Two-Moment Bulk Stratiform Cloud Microphysics Scheme in the Community Atmosphere Model, Version 3 (CAM3). Part I: Description and Numerical Tests, *Journal of Climate*, *21*(15), 3642–3659, doi:10.1175/2008JCLI2105.1.

Pincus, R., and S. A. Klein (2000), Unresolved spatial variability and microphysical process rates in large-scale models, *J. Geophys. Res.*, *105*(D22), 27059–27,065, doi:10.1029/2000JD900504.

Pincus, R., S. A. McFarlane, and S. A. Klein (1999), Albedo bias and the horizontal variability of clouds in subtropical marine boundary layers: Observations from ships and satellites, *J. Geophys. Res.*, *104*(D6), 6183–6191, doi:10.1029/1998JD200125.

Suzuki, K., T. Y. Nakajima, and G. L. Stephens (2010), Particle Growth and Drop Collection Efficiency of Warm Clouds as Inferred from Joint CloudSat and MODIS Observations, *Journal of the Atmospheric Sciences*, *67*(9), 3019–3032, doi:10.1175/2010JAS3463.1.

Wood, R., and D. L. Hartmann (2006), Spatial Variability of Liquid Water Path in Marine Low Cloud: The Importance of Mesoscale Cellular Convection, *Journal of Climate*, *19*(9), 1748–1764, doi:10.1175/JCLI3702.1.